

Supplementary data

Biodegradable Organosilica Magnetic Micelles for Magnetic Targeting MRI and GSH-triggered Tumor Chemotherapy

Tiangang Yang, Dechao Niu,* Jianzhuang Chen, Jianping He, Shaobo Yang, Xiaobo Jia, Jina Hao, Wenru Zhao and Yongsheng Li,*

Lab of Low-Dimensional Materials Chemistry, Key Laboratory for Ultrafine Materials of Ministry of Education, School of Materials Science and Engineering, East China University of Science and Technology, Shanghai 200237, China. E-mail: dcniu@ecust.edu.cn; ysli@ecust.edu.cn.

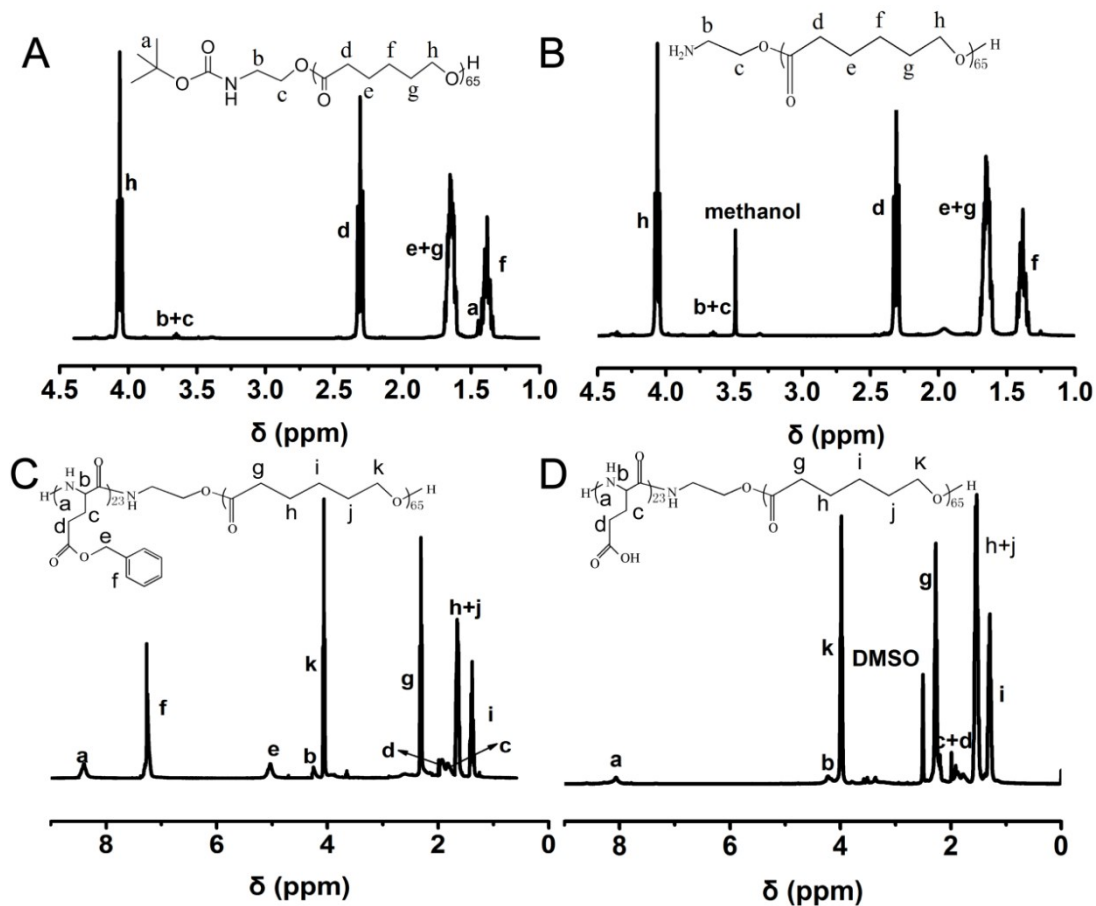


Fig. S1. ^1H NMR spectra of (A) PCL₆₅-NH-Boc in CDCl₃, (B) PCL₆₅-NH₂ in CDCl₃ (C) PCL₆₅-b-PBLG₂₃ in DMSO-*d*₆ and (D) PCL₆₅-b-PGA₂₃ in DMSO-*d*₆.

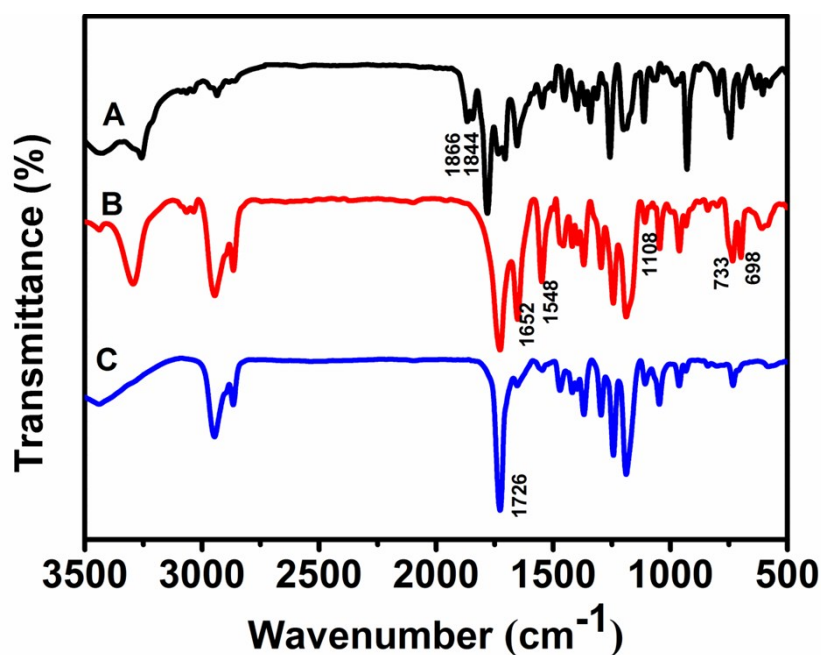


Fig. S2. FT-IR spectra of (A) Bz-Glu NCA, (B) PCL₆₅-b-PBLG₂₃ and (C) PCL₆₅-b-PGA₂₃.

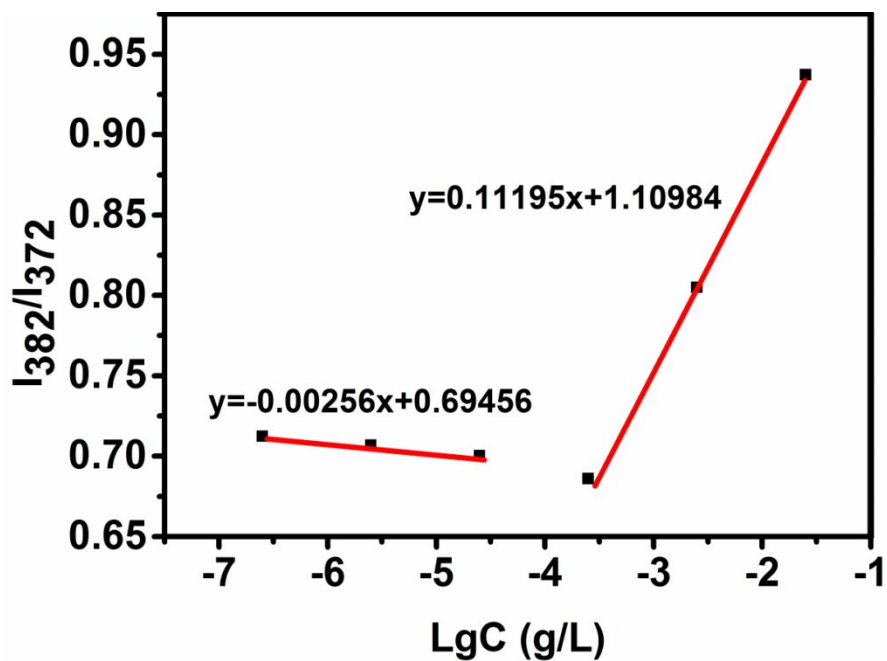


Fig. S3. The critical micelle concentration (CMC) of PCL₆₅-b-PGA₂₃.

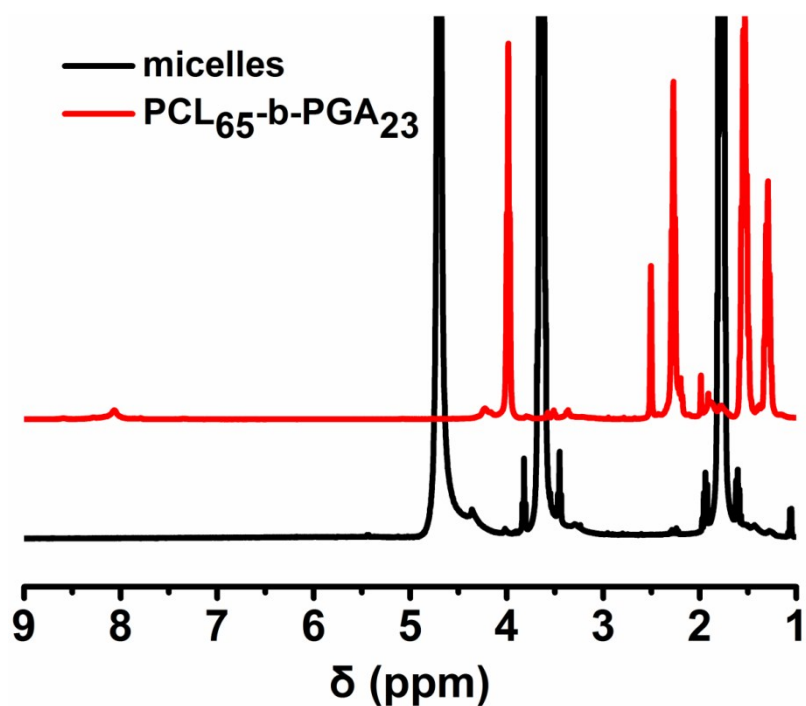


Fig. S4. ¹H NMR spectra of PCL₆₅-b-PGA₂₃ in DMSO-*d*₆ and the micelles self-assembled from PCL₆₅-b-PGA₂₃ in D₂O.

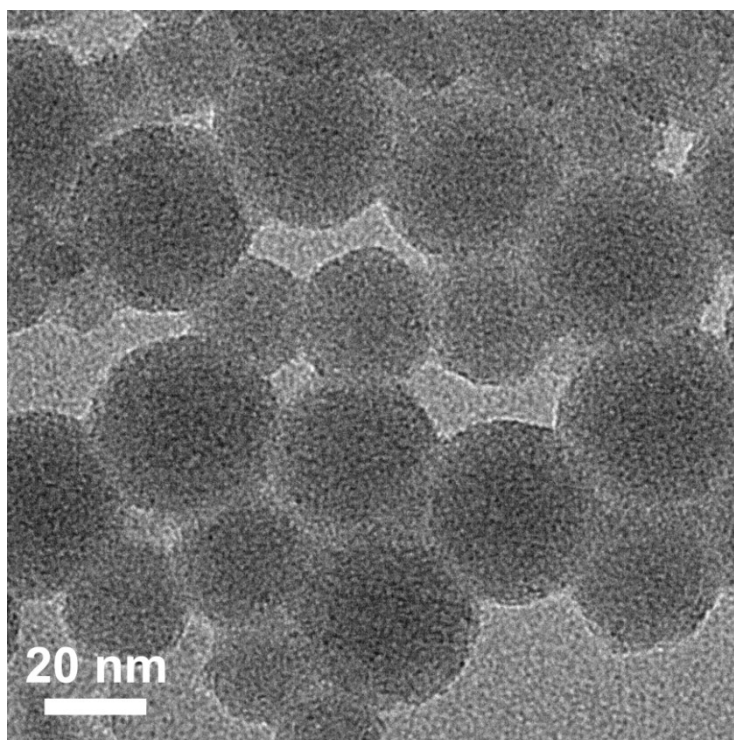


Fig. S5. TEM image of organosilica micelles after calcination at 450 °C for 6 h.

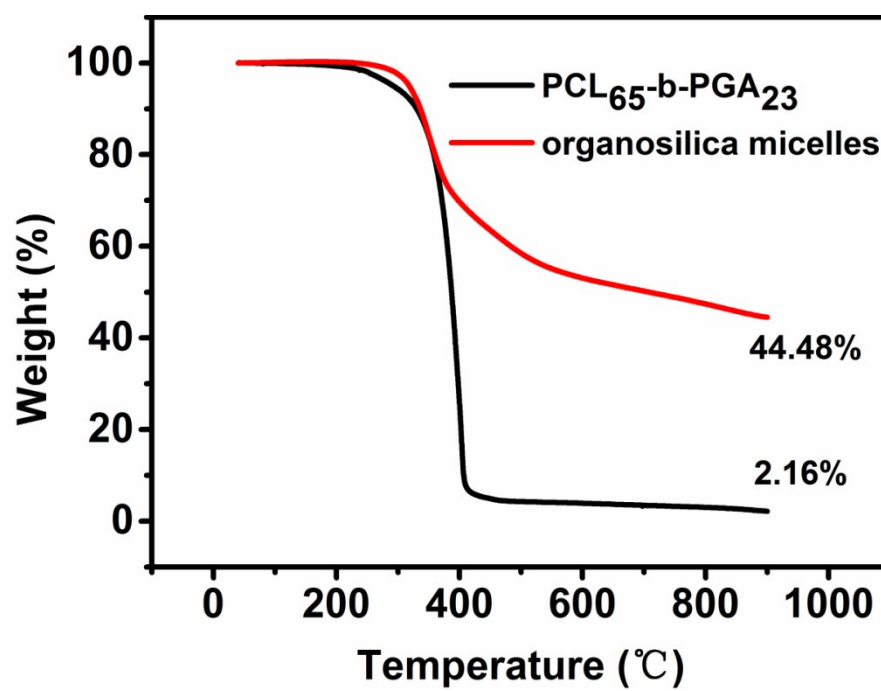


Fig. S6. TG curves of PCL₆₅-b-PGA₂₃ and organosilica PCL₆₅-b-PGA₂₃ micelles.

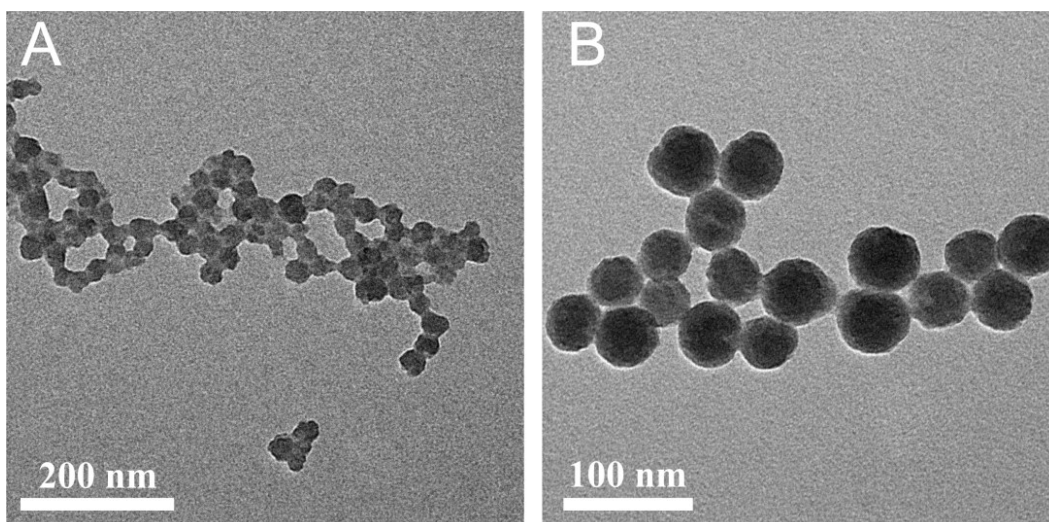


Fig. S7. TEM images of organosilica micelles synthesized using different amounts of MPTMS. (A) 50 μL and (B) 150 μL .

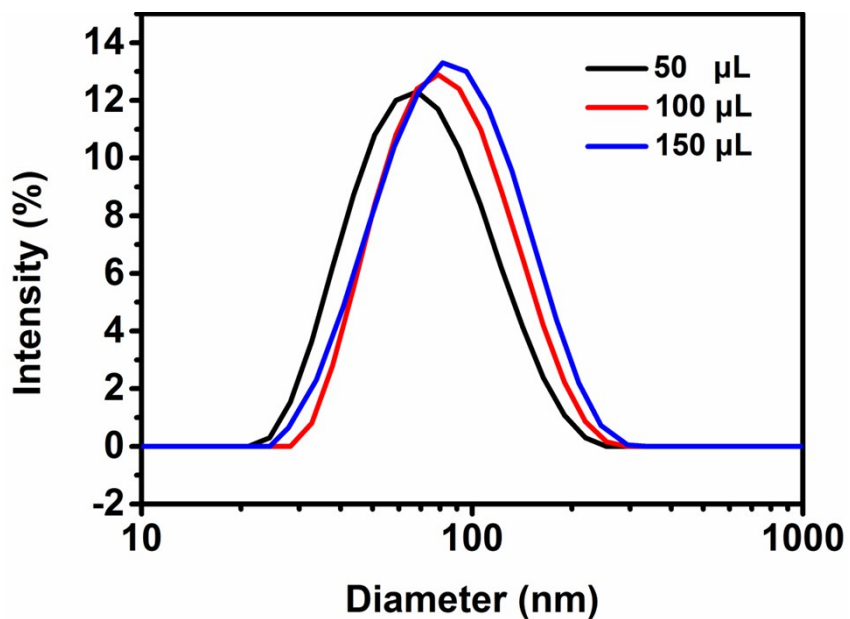


Fig. S8. Hydrodynamic size distributions of organosilica micelles prepared with different amounts of MPTMS (measured in water).

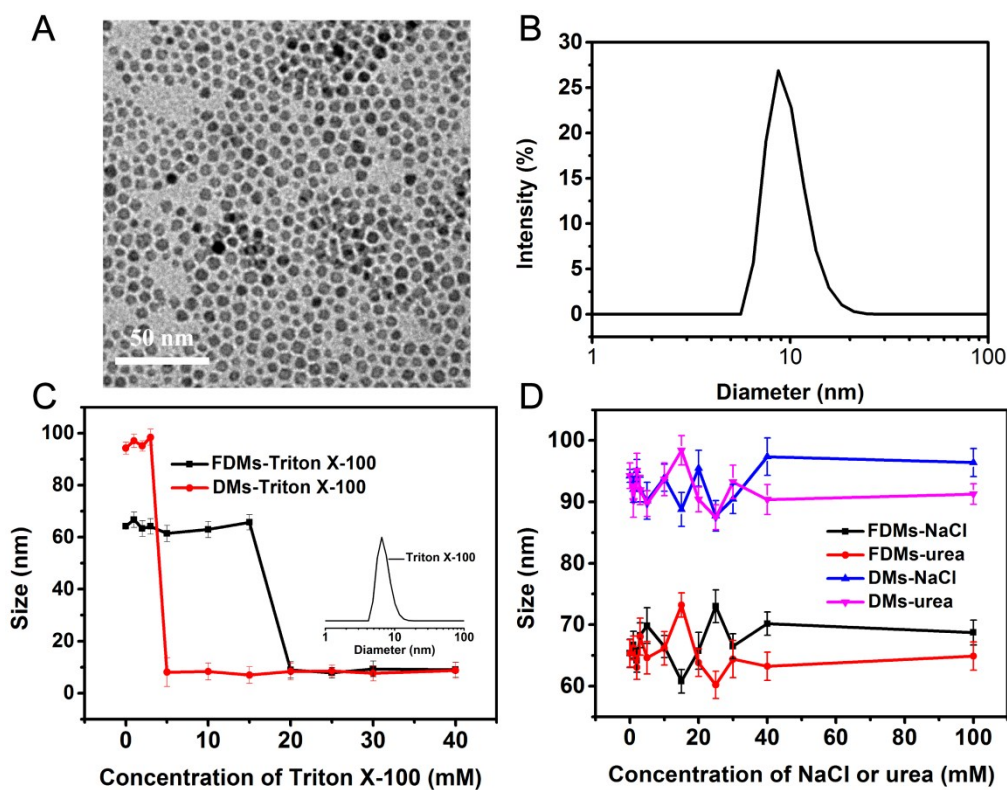


Fig. S9. (A) TEM image and (B) size distribution of hydrophobic Fe_3O_4 in THF solvent. The size changes of FDMs and DMs in water after treatment with different concentrations of (C) Triton X-100, (D) NaCl and urea, respectively. (The inset in C is the size distribution of Triton X-100 micelles self-assembled in H_2O).

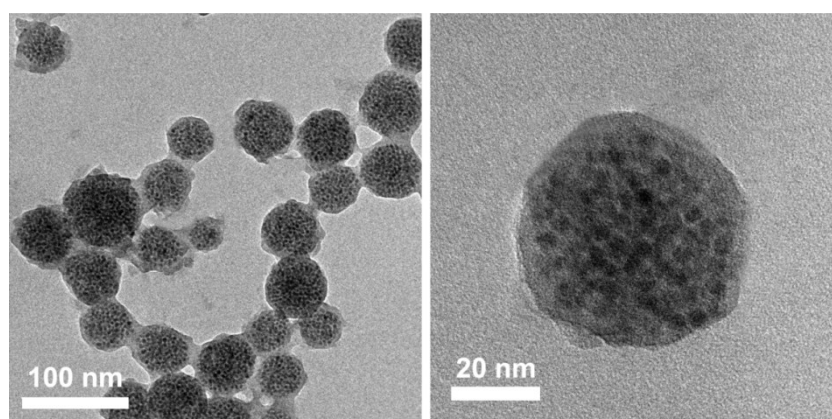


Fig. S10. TEM images of FOMs prepared by using $10 \mu\text{L}$ of MPTMS .

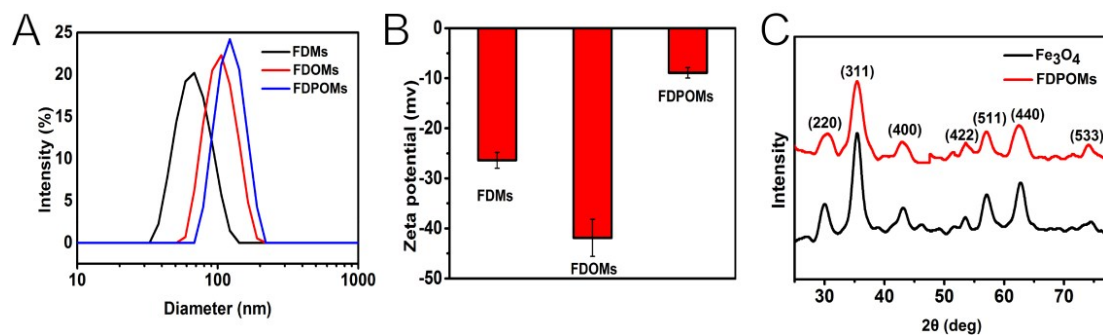


Fig. S11. (A) Size distributions and (B) Zeta potentials of FDMs, FDOMs and FDPOMs in water. (C) XRD patterns of Fe₃O₄ nanoparticles and FDPOMs.

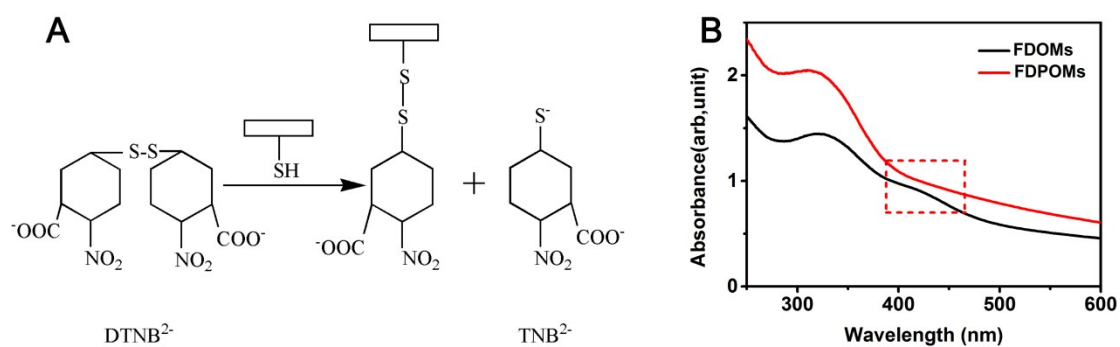


Fig. S12. (A) Schematic illustration of the reaction between Ellman's reagent and thiols. (B) UV-vis spectra of Ellman's reagent mixed with FDOMs and FDPOMs, respectively.

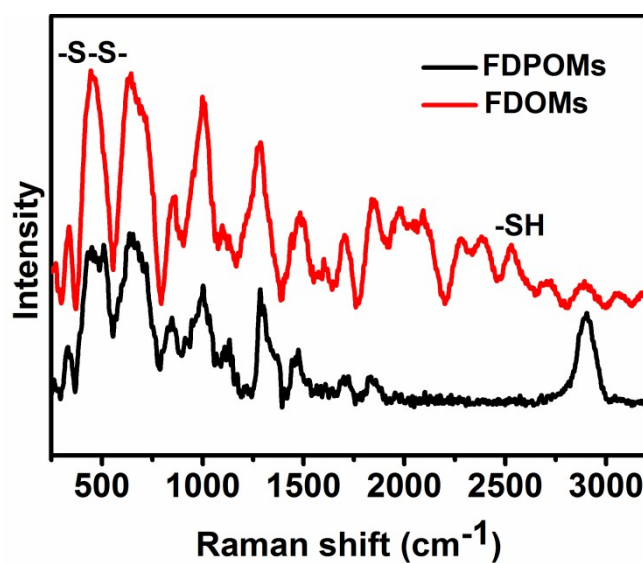


Fig. S13. Raman spectra of FDOMs and FDPOMs.

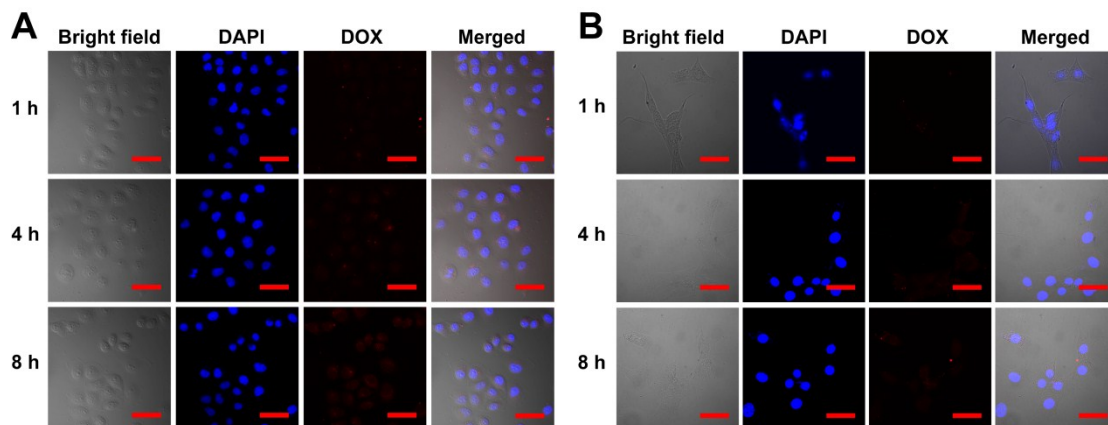


Fig. S14. CLSM images of intracellular DOX for (A) SMMC-7721 cancer cells and (B) 3T3 normal cells incubated with FDPOMs for 1, 4, and 8 h. The scale bars are 50 μm.

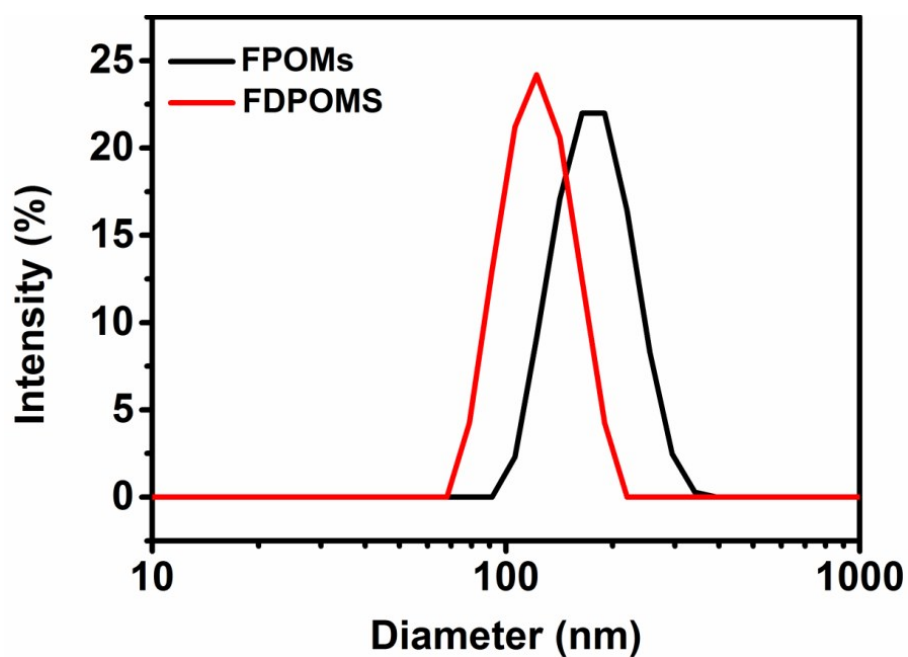


Fig. S15. Dynamic-diameters distributions of FPOMs and FDPOMs in water.

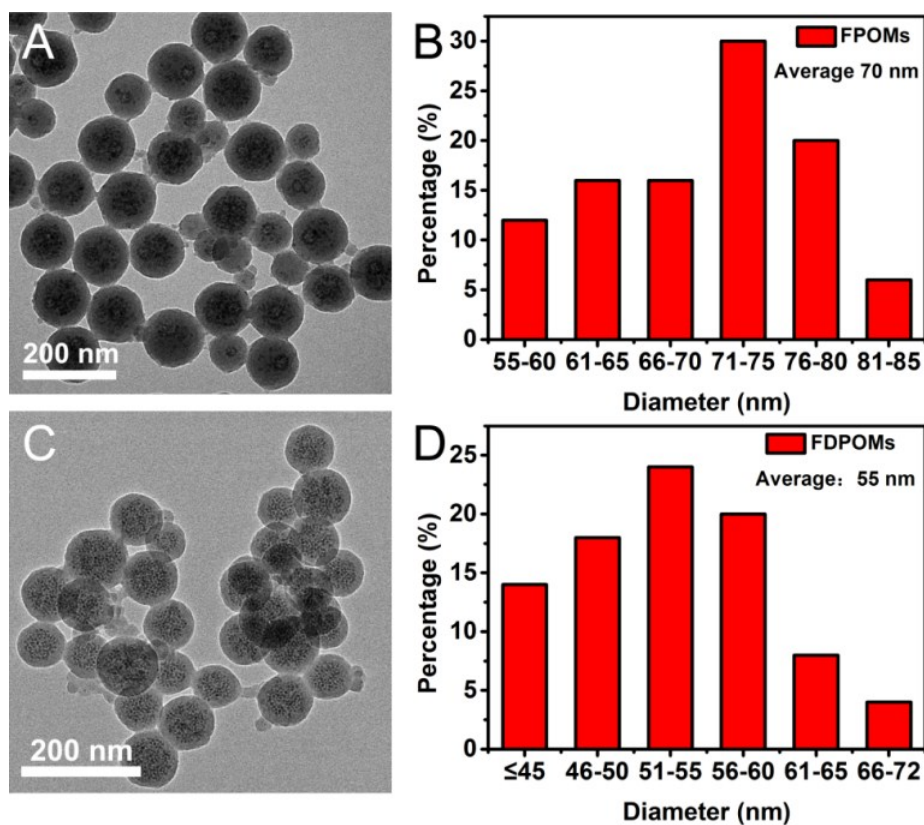


Fig. S16. TEM images (A, C) of FPOMs and FDPOMs and corresponding size distributions (B, D) of magnetic clusters by measuring 50 particles from TEM images of FPOMs and FDPOMs.

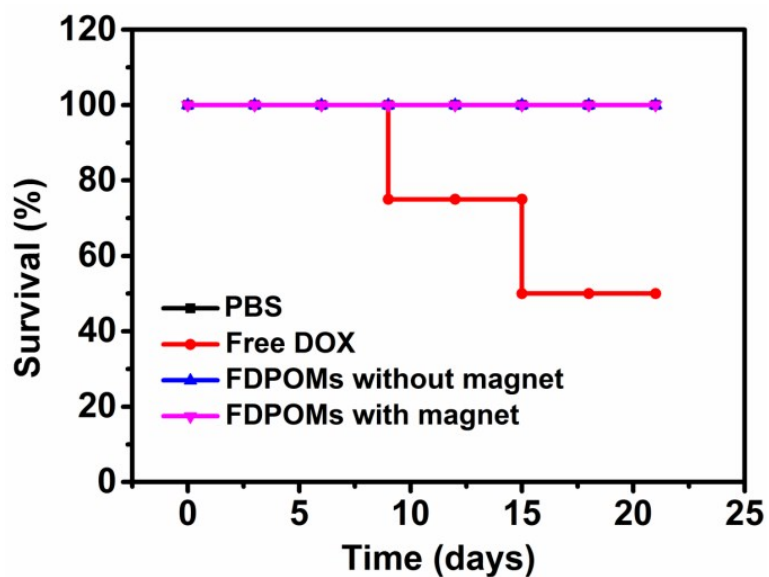


Fig. S17. Survival rates of SMMC-7721 tumor-bearing mice after intravenous injection of different formulations.

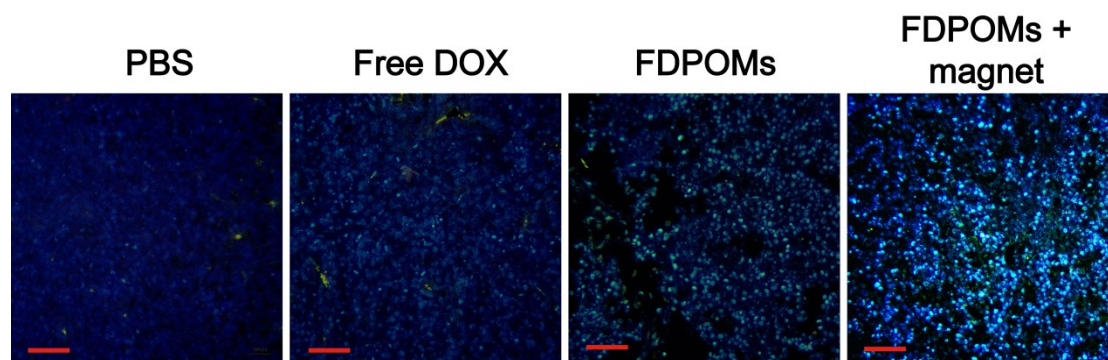


Fig. S18. TUNEL immunofluorescence staining images of tumor slices from mice treated with PBS, free DOX and FDPOMs with or without magnet. The scale bars are 200 μm .